

# Strain Range Dependence of Young's Modulus and Size Effects of Mechanical Properties for Chiral Graphene by Molecular Dynamics Simulations

Yi-Xiu Du

Tianjin University of Technology and Education

Li-Jun Zhou (✉ [zhoulj\\_tj@163.com](mailto:zhoulj_tj@163.com))

Tianjin University of Technology and Education

Jian-Gang Guo

Tianjin University

---

## Research Article

**Keywords:** Graphene, Molecular dynamics simulations, Strain range dependence, Size effects

**Posted Date:** September 20th, 2021

**DOI:** <https://doi.org/10.21203/rs.3.rs-748572/v1>

**License:**  This work is licensed under a Creative Commons Attribution 4.0 International License.

[Read Full License](#)

---

# Strain range dependence of Young's modulus and size effects of mechanical properties for chiral graphene by molecular dynamics simulations

Yi-Xiu Du<sup>a</sup>, Li-Jun Zhou<sup>a,\*</sup>, Jian-Gang Guo<sup>b</sup>

<sup>a</sup>Department of Mechanical Engineering, Tianjin University of Technology and Education, Tianjin 300222, China

<sup>b</sup>Tianjin Key Laboratory of Modern Engineering Mechanics, School of Mechanical Engineering, Tianjin University, Tianjin 300072, China

## Abstract

The stress-strain response of pristine monolayer graphene under uniaxial loading/unloading over a larger size range (100nm×100nm) is studied by molecular dynamics (MD) simulations, which proves that graphene is perfectly elastic prior to the failure strain. Young's modulus of graphene is calculated by selecting different strain ranges in the elastic region. It is found that Young's modulus is strongly dependent on the strain range. When the selected strain ranges are increased from 0.5% to 8%, Young's modulus of the armchair and zigzag graphene is reduced by approximately 60 Gpa and 150 Gpa, respectively. Based on the Pearson correlation coefficient method, the linearity of the stress-strain curve during graphene stretching is studied. The elastic region of the tensile curve is divided into the linear elastic region and non-linear elastic region. simultaneously, the linear elastic limit strains for the armchair and zigzag graphene are defined to be about 2.5% and 1.5%, respectively, and they are independent of the size of graphene. On this basis, the chirality dependence and size effects of Young's modulus, failure strain, and fracture strength of pristine monolayer graphene are investigated. The results show that Young's modulus is dependent on the chiral angle but insensitive to size. The failure strain and fracture strength depend on the chiral angle and have obvious size effects, which decrease with the increase of size range and size ratio.

**Keywords:** Graphene; Molecular dynamics simulations; Strain range dependence; Size effects

## Introduction

Graphene, defined as the two-dimensional nanomaterials of honeycomb lattice with carbon atoms [1], has broad application prospects [2-3] in the fields of nanodevices, flexible electronics, nanocomposites due to its exceptional mechanical properties [4-5]. Young's modulus of graphene is a crucial indicator to measure its mechanical properties. Therefore, to obtain reliable and accurate Young's modulus has great significance for understanding its mechanical properties in depth.

So far, a large number of studies on the elastic properties of graphene have been carried out via nanoindentation experiments in atomic force microscope [4], continuum elasticity theory [6] as well as molecular dynamics simulations [7-9]. The results show that graphene exhibits nonlinear elasticity under tensile loading. Hence, it is necessary to select a certain strain range in the stress-strain curve to form an equivalent linear elastic region to fit it when calculating Young's modulus of graphene. Mortazavi et al. [10] and Zhao et al. [11] both selected a small strain range (<0.5%) as a linear elastic region and calculated Young's modulus of graphene based on molecular dynamics

---

\* Corresponding author: L.-J. Zhou; Email: [zhoulj\\_tj@163.com](mailto:zhoulj_tj@163.com).

simulations. Zhang et al. [12] calculated Young's modulus of graphene by taking the strain range less than 2% as the linear elastic region. Meanwhile, Pei et al. [13] linearly fitted Young's modulus in the strain range of 3%. Sun et al. [14] believed that the stress increases linearly with the strain till 8% and calculated Young's modulus in the strain range of 8%. Moreover, Wang et al. [15] proposed that the initial deformation with a small strain can be regarded as a linear elastic region to fit. Thus, in the current studies, a unified strain range has not been selected to define the linear elastic region of graphene in the calculation of Young's modulus.

Recently, the strain dependence of graphene elastic properties has been reported in some researches. López-Polín et al. [16] measured Young's modulus of unstrained and strained graphene by indentation experiments, and found that Young's modulus of graphene with strain (0.25%) was significantly improved. By Raman spectroscopy measurement technology, Androulidakis et al. [17] investigated the effect of strain on Young's modulus for graphene. The researches showed that when graphene was compressed, Young's modulus was strongly dependent on strain in the strain range of -0.6%, while when graphene was stretched, the stress increased linearly with strain in the strain range of 1.5%. Prabhakar et al. [18] and Qu et al. [19] found that Young's modulus exhibits nonlinear behavior with strain using first-principles and density functional theory calculations, respectively. Moreover, it firstly increases as increasing strain and then sharply decreases. Los et al. [20] considered the in-plane Young's modulus to be dependent on the strain by using atomistic Monte Carlo simulations. Hosseini Kordkheili et al. [21] proved by finite element method that Young's modulus depends on the strain and decreases linearly with the increase of strain. In conclusion, it has been discovered that Young's modulus of graphene is strongly dependent on the strain, so it is difficult to obtain a reliable and accurate Young's modulus value by selecting different strain regions to fit Young's modulus.

Besides, the related investigations have also indicated that Young's modulus, failure strain, and fracture strength of graphene exhibit size effects. Based on the finite element method [22,24], molecular dynamics simulations [11,25], and first-principles calculations [19], respectively, it was found that Young's modulus is dependent on the size ratio in the size range (15nm×15nm) with altering its size ratio. Similarly, Georgantzinos et al. [23] also discovered that the failure strain and fracture strength are dependent on the size ratio. Meanwhile, As the size ratio is 1 with changing the size range of graphene, the size range dependence of Young's modulus was studied by molecular dynamics simulations [8,26]. Ni et al. [8] found that it is not sensitive to the size range. While Chen et al. [26] considered that Young's modulus, failure strain, and fracture strength have size range effects in a smaller strain range. Therefore, there are some contradictory conclusions in the present researches. In addition, the investigations on size effects of Young's modulus, failure strain, and fracture strength are mainly focused on the graphene with a smaller size range [20,27-28], and relatively few studies on a larger size range.

In this paper, the stress-strain response of the armchair and zigzag graphene during uniaxial loading/unloading in a larger size range (100nm×100nm) is studied by means of molecular dynamics simulations. Young's modulus of graphene is calculated by selecting different strain ranges in the elastic region. Based on the Pearson correlation coefficient method, the linearity of the stress-strain curve under graphene stretched is studied. The elastic region of the tensile curve is divided into the linear elastic region and nonlinear elastic region, and the linear elastic limit strains applied in the armchair and zigzag graphene are defined regardless of size. On this basis, the chirality-dependence and size effects of Young's modulus, failure strain, and fracture strength of

pristine monolayer graphene are studied.

## Models and methods

### Models of chiral graphene

The armchair and zigzag monolayer pristine graphene models are illustrated in Fig.1, where  $L$  and  $W$  are the length and width of graphene. A uniaxial load is applied to the carbon atoms at the boundary along the X (armchair)-directions and Y(zigzag)-directions.

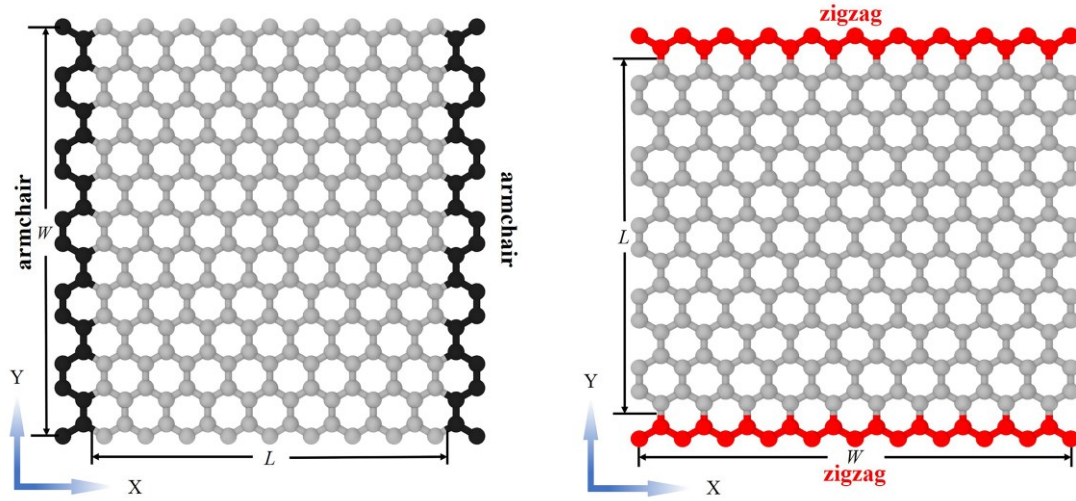


**Fig. 1** The schematics of the armchair and zigzag monolayer pristine graphene.

The defined lattice vector  $a_1(x_1, y_1)$  and  $a_2(x_2, y_2)$  rotate a certain angle  $\alpha$  clockwise around the origin of the coordinates in the two-dimensional plane rectangular coordinates systems (fig. 2), the following expressions of new coordinate corresponding to the rotation of  $a_1(x_1, y_1)$  can be derived:

$$\begin{cases} x = x_1 \cos \alpha + y_1 \sin \alpha \\ y = y_1 \cos \alpha - x_1 \sin \alpha \end{cases} \quad (1)$$

The  $\alpha$  is defined as the chiral angle of graphene, which can be specified as  $0^\circ$ ,  $3^\circ$ ,  $9^\circ$ ,  $15^\circ$ ,  $21^\circ$ ,  $27^\circ$ ,  $30^\circ$  in the simulations, where  $0^\circ$  is along the zigzag direction and  $30^\circ$  along the armchair direction considering the periodic structure of graphene [29-30].

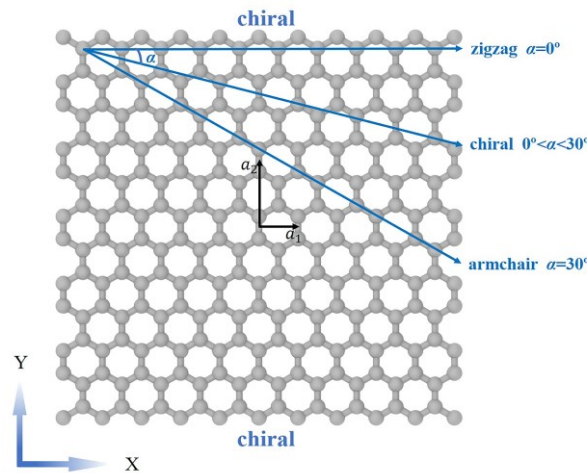


**Fig. 2** Chiral angle of graphene.

## Simulation method and process

Molecular dynamics simulations are performed using AIREBO [31] (adaptive intermolecular reactive bond order) potential function to describe the interactions between carbon atoms in graphene. In order to avoid spuriously high forces of the carbon-carbon covalent bond, which can arise nonphysical explanations, we set the onset of the covalent interaction cutoff distance to be 2.0Å in the AIREBO potential [32]. The temperature at 0.1K is applied using the Nose-Hoover thermostat to avert complex effects caused by the thermal activation of atoms [14-15]. Before the simulations of loading/unloading about graphene of the different sizes, the periodic boundary conditions are set in the loading/unloading direction. The graphene is stretched after unconstrained relaxation by moving the boundary at the engineering strain rate (0.1%) with a timestep of 0.001ps, and strain increment is applied every certain relaxation steps until the failure strain [33]. Furthermore, moving the boundary at the adverse engineering strain rate (-0.1%) to simulate the unloading process in the same way [34]. Fig.3 presents the variation of total energy with unconstrained relaxation steps in a graphene model (15nm×15nm). The initial steps at which the total energy of graphene to attain a stable value are chosen, not only ensures that graphene lies in the lowest energy equilibrium state but also avoids the dynamic instability suffer from the violent fluctuation of graphene edges because of excessive relaxation time [35]. In addition, the longer unconstrained relaxation steps of total energy attain a stable value with the size of graphene and carbon atoms increase, the longer of relaxation steps during loading/unloading. Therefore, references of nine models of different sizes towards unconstrained relaxation steps and loading/unloading relaxation steps are listed in table 1.

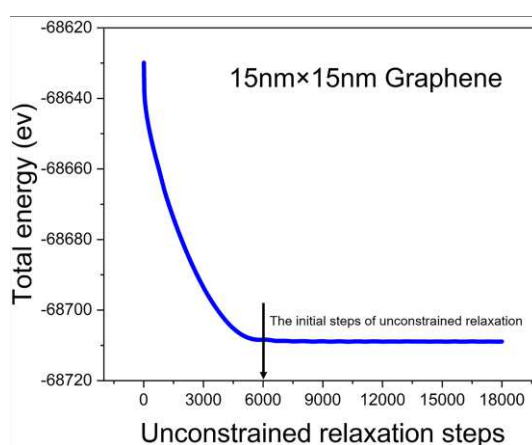


**Fig. 3** Variation of total energy with unconstrained relaxation steps.

**Table 1**

References of unconstrained relaxation steps and loading/unloading relaxation steps.

The model number	$L/nm$	$W/nm$	atoms	Unconstrained relaxation steps	Loading/unloading relaxation steps
1	2.41	2.58	260	1600	150
2	5.07	5.09	1000	2200	175
3	10.15	10.11	3900	4500	225
4	14.98	15.14	8800	6000	350
5	20.08	20.16	15600	7500	475
6	24.92	25.18	25000	9000	625

7	30.00	30.21	35000	11000	775
8	50.09	49.89	99800	11800	1350
9	100.17	100.14	390000	36000	2800

## Results and discussion

### Elastic properties of graphene

The stress of graphene during uniaxial loading/unloading is calculated according to the virial theorem theory [36-37]. For the armchair and zigzag graphene, the stress-strain curves are illustrated in Fig.4, respectively, when the graphene is loaded to complete fracture within a larger size range (100nm×100nm). It is not difficult to see that the stress increases nonlinearly with the strain. Fig.5 shows the whole loading and unloading stress-strain curves before the fracture point under a size range (15nm×15nm) for two types of chiral graphene. It can be seen from this figure that the whole loading and unloading stress-strain curves almost overlap, which indicates graphene maintains elastic deformation under the loading process before the failure strain. Hence, we consider the whole loading process before fracture strain as the nonlinear elastic region.

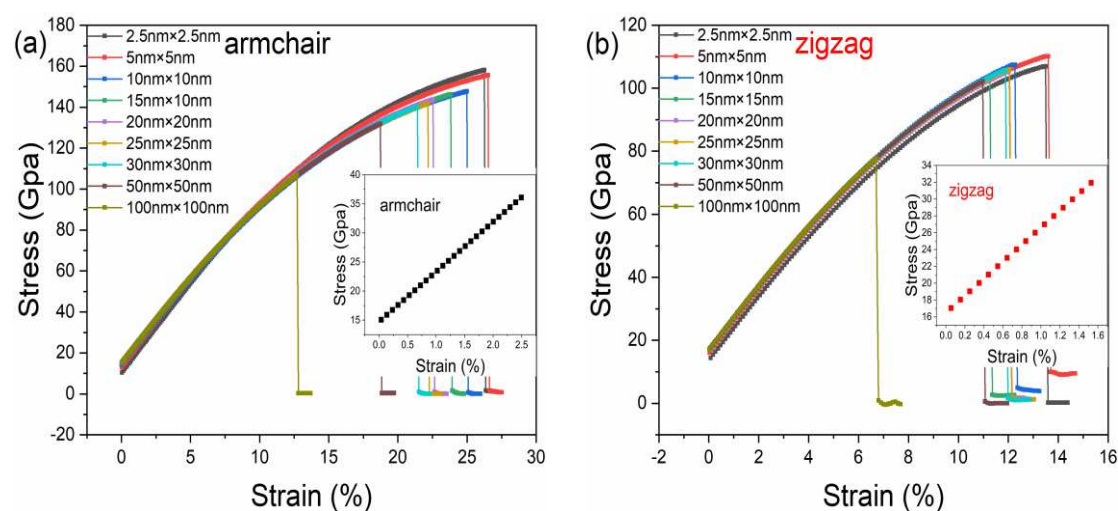


**Fig. 4** Stress-strain curves of graphene with different sizes (a)armchair (b)zigzag.

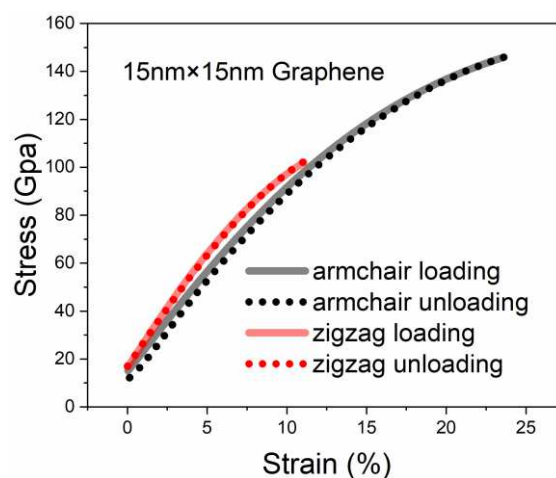


**Fig. 5** Loading/unloading stress-strain curves of the armchair and zigzag graphene.

## Strain range dependence of Young's modulus

Young's modulus of graphene is calculated by selecting a strain range that can be equivalent to a linear elastic region and fitted by the least square method. The strain ranges selected in Fig.6 start from (0~0.5%) and continue to increase to (0~8%) at a tensile strain rate of 0.1%. Fig.6 shows the variations of Young's modulus with the strain range applied in the armchair and zigzag, and it can be found that Young's modulus has a strong dependence on the strain range. Meanwhile, Young's modulus decreases obviously with the increase of selected strain ranges. Young's modulus is fitted from different strain ranges for the armchair and zigzag graphene are listed in table.2 and table.3, respectively. The calculated results are similar to Young's modulus attained by selecting the same strain range reported in the piece of literature [10-11, 13-14, 17, 38]. We can find from Table.2 and 3 that Young's modulus of the armchair and zigzag decrease about 60 Gpa and 150 Gpa, respectively when the strain ranges increase from 0.5% to 8%. However, when the selected strain ranges of the armchair and zigzag are less than 2.5% and 1.5%, respectively, the variations of Young's modulus are only about 5Gpa. In other words, the dependence of Young's modulus for graphene on the strain ranges is significantly reduced, and the linear coincidences degree of the stress-strain curve is better.

To prove it, the Pearson correlation coefficient method is further applied to study the linearity of the stress-strain curve. Table.4 lists the strain range of the stress-strain curve with Pearson's correlation coefficient equal to 1 applied in the armchair and zigzag graphene of different sizes. That is, stress is completely linearly related to strain. The data indicates that the stress and strain have preferable linearity coincidences in the strain range of 2.5% and 1.5% applied in the armchair and zigzag graphene, respectively.

Based on the above analysis, we divide the elastic region of the tensile curve into the linear elastic region and non-linear elastic region, and define the linear elastic limit strains for the armchair and zigzag graphene to be about 2.5% and 1.5% regardless of size, as shown in insets of fig.4(a) and fig.4(b). Moreover, the linear elastic limit strains defined above have a reasonable agreement with the linear elastic region of graphene in the stress-strain curve by experimental measurement [17,38].

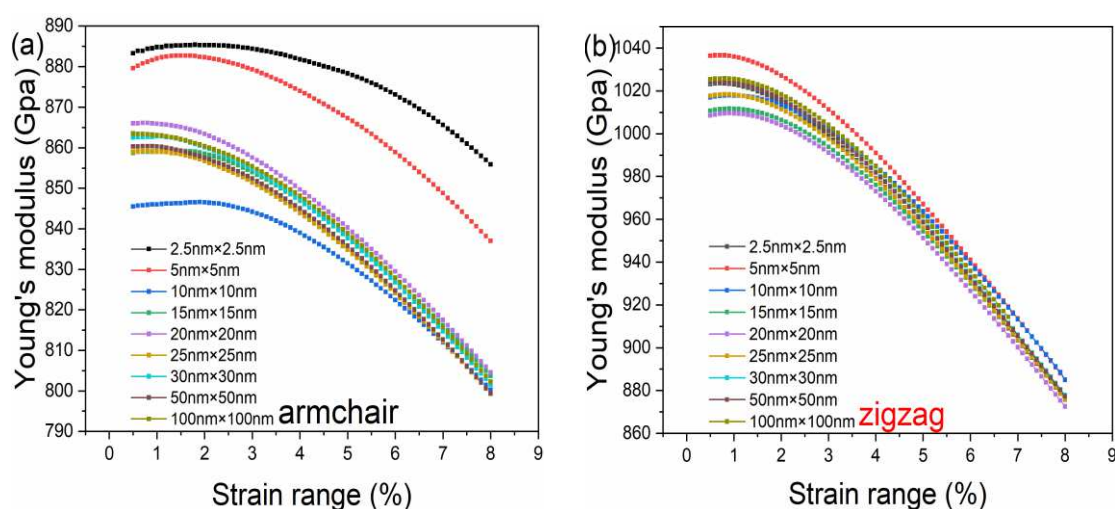


**Fig. 6** Variations of Young's modulus with different strain ranges (a)armchair (b)zigzag.

**Table 2**

The fitted Young's modulus of the armchair graphene by selecting different strain ranges.

The model number (armchair)	Young's modulus (Gpa)					
	0.5%	1.5%	2.5%	3%	5%	8%
1	883.3	885.2	885.1	884.4	878.3	855.9
2	879.6	882.7	881.1	879.3	867.3	837
3	845.5	846.3	845.8	844.2	831.5	800.3
4	858.7	859.3	856.6	854	838	803.7
5	866	865.1	860.8	857.6	840.3	804.6
6	859	858.4	854.3	851.4	834.8	799.3
7	862.5	862	857.7	854.7	837.7	801.6
8	860.3	859.3	855.3	852.4	835.8	799.4
9	863.5	862.1	858.2	855.4	838.9	802.3

**Table 3**

The fitted Young's modulus of the zigzag graphene by selecting different strain ranges.

The model number (zigzag)	Young's modulus (Gpa)					
	0.5%	1.5%	2.5%	3%	5%	8%
1	1023.1	1019.8	1007.4	999	955.8	875.8
2	1036.4	1032.7	1019.9	1011.3	967.1	885
3	1017	1016.6	1008.4	1001.9	963.7	885
4	1010.7	1010.1	1000.9	993.8	954.4	876.6
5	1008.5	1007.9	998.2	991.1	951.2	872.6
6	1017.6	1015.9	1005.2	997.6	956	875.9
7	1023.9	1020.9	1009.5	1001.5	958.9	877.8
8	1024.1	1021	1009.4	1001.3	958.5	877.3
9	1025.3	1023	1011.9	1004	961.5	—

**Table 4**

The strain range of the stress-strain curves for the armchair and zigzag graphene with Pearson's correlation coefficient equal to 1.

The model number	Pearson's correlation coefficient $r=1$	Pearson's correlation coefficient $r=1$
	(armchair)	(zigzag)
1	4%	1.5%
2	3.1%	1.5%
3	3.2%	1.9%
4	2.6%	1.8%
5	2.3%	1.8%
6	2.4%	1.7%

7	2.3%	1.6%
8	2.4%	1.6%
9	2.4%	1.7%

### Size effects of mechanical properties

On this basis, Young's modulus of the armchair and zigzag graphene with different sizes are calculated by using the defined strain region of linear elasticity. The variations of Young's modulus for graphene with the size range are illustrated in fig.7. when the size ratio of graphene is 1, The results manifest that Young's modulus of the armchair is less than zigzag, and Young's modulus of two types of chirality is insensitive to the size range. Fig.8 shows the variations of Young's modulus for graphene with size ratio,  $W/L$  or  $L/W$ , by keeping its length or width constant, i.e.,  $L=5\text{nm}$  or  $W=5\text{nm}$ . When the length is constant, Young's modulus of the armchair and zigzag tend to be stable as the size ratio increases. When the width is constant, Young's modulus shows a decreasing trend as the size ratio  $L/W$  increases and tends to be stable as the size ratio  $L/W$  greater than 8. Therefore, it can be concluded that the dependence of Young's modulus for graphene on the size range and size ratio is not obvious.

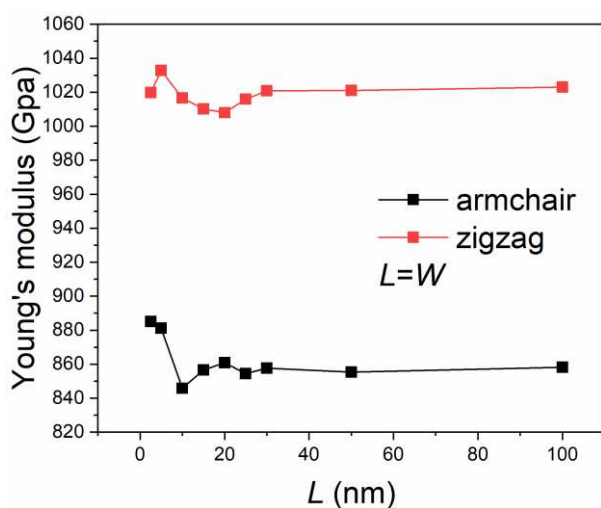


**Fig. 7** Variations of Young's modulus for the armchair and zigzag graphene with increasing the size range.

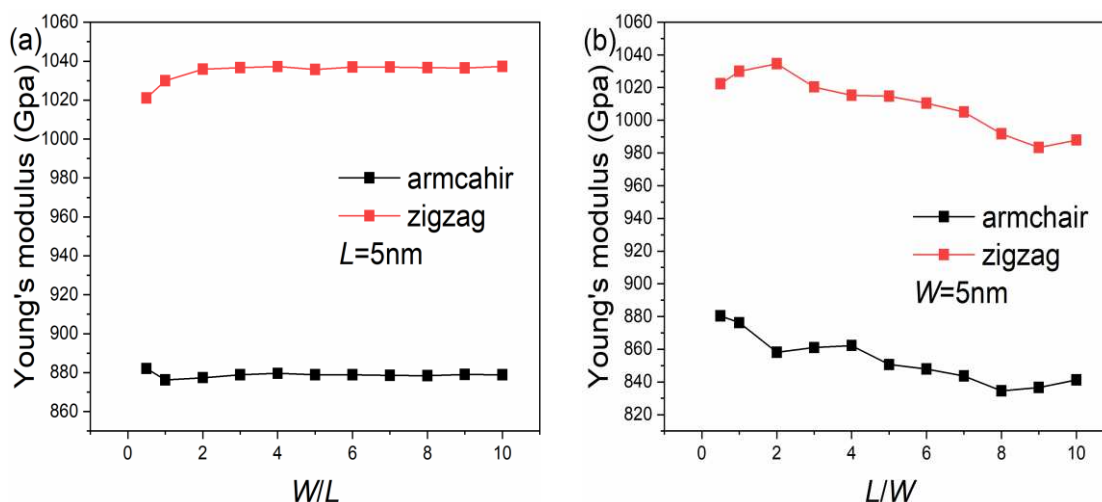
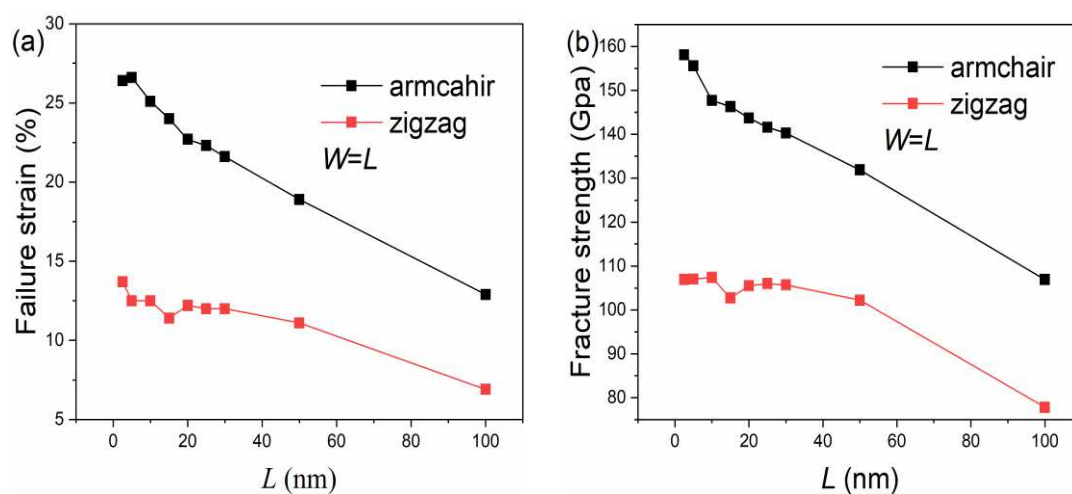


**Fig. 8** Variations of Young's modulus of the armchair and zigzag graphene with size ratio (a)  $W/L$  (b)  $L/W$ .

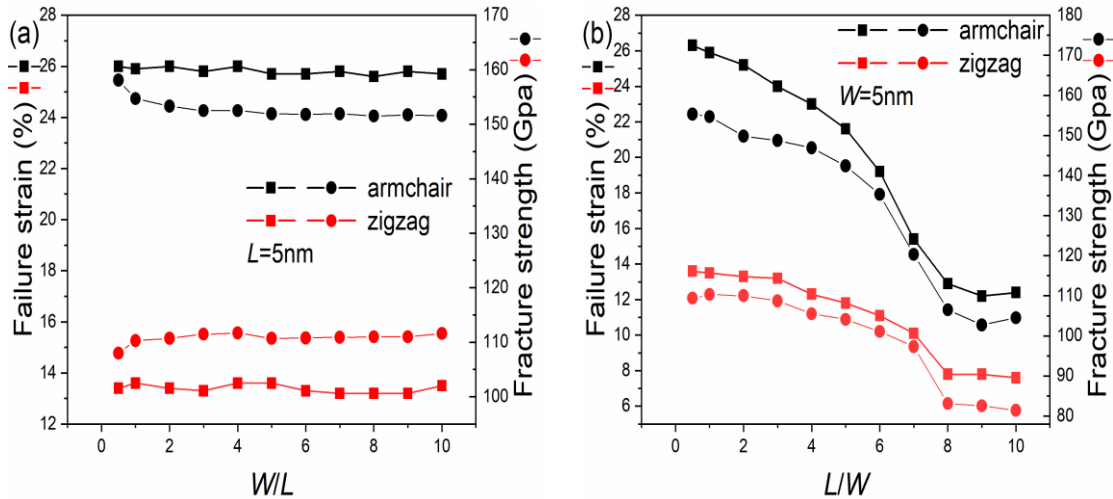
The variations of failure strain and fracture strength for graphene with the size range are shown in Fig.9. Obviously, the failure strain and fracture strength of the armchair are greater than those of zigzag. Moreover, the failure strain and fracture strength are both dependent on the size range of graphene and decrease with increasing the size range of graphene.

Fig.10 shows the variations of failure strain and fracture strength for graphene with size ratio,  $W/L$  or  $L/W$ , by keeping its length or width constant, i.e.,  $L=5\text{nm}$  or  $W=5\text{nm}$ . It can be found that failure strain and fracture strength of the two types of chirality tend to be stable as the size ratio  $W/L$  increases. Meanwhile, they show a decreasing trend as the size ratio  $L/W$  increases and tend to be stable as the size ratio  $L/W$  is greater than 8.

Based on the above analysis about the variations of failure strain and fracture strength with size range and size ratio, we can conclude that the failure strain and fracture strength for graphene have noticeable size effects. The failure strain and fracture strength of graphene are more sensitive to length than width.



**Fig. 9** Variations of (a) failure strain and (b) fracture strength for graphene with increasing the size range.



**Fig. 10** Variations of failure strain and fracture strength for graphene with size ratio (a)  $W/L$  (b)  $L/W$ .

### Chiral angle dependence of mechanical properties

The mechanical properties of the armchair and zigzag graphene are different, so it can be concluded that the mechanical properties of graphene are chiral-angle-dependent. According to the chiral angle defined in the 2.1 section, Young's modulus, failure strain, and fracture strength are calculated when the chiral angles are equal to  $0^\circ$ ,  $3^\circ$ ,  $9^\circ$ ,  $15^\circ$ ,  $21^\circ$ ,  $27^\circ$  and  $30^\circ$ , respectively. The results are illustrated in Fig. 11. Some interesting phenomena can be drawn from these figures. In Fig. 11(a), Young's modulus reaches its maximum at  $3^\circ$ . When the zigzag graphene ( $0^\circ$ ) rotates clockwise to a certain angle to the armchair graphene ( $30^\circ$ ), Young's modulus shows a decreasing trend with the increase of chiral angle. In addition, the values of Young's modulus for other chiral angles are basically between those of the armchair and zigzag. The chiral angle dependence of failure strain and fracture strength are shown in Fig. 11(b) and Fig. 11(c), respectively. It can be found that failure strain and fracture strength reach minimum values when the chiral angle is  $20^\circ$ . What's more, failure strain and fracture strength reduce gradually as the chiral angle is less than  $20^\circ$ , and then rapidly increase as they are greater than  $20^\circ$  [39-41].

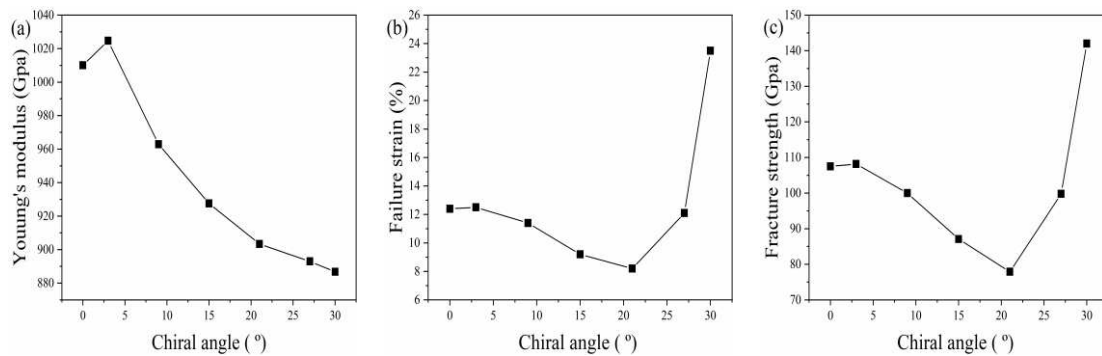


**Fig. 11** Chiral angle dependence of (a) Young's modulus (b) failure strain and (c) fracture strength.

## Conclusions

The stress-strain response of the armchair and zigzag graphene during uniaxial loading/unloading in a larger size range (100nm×100nm) is investigated by means of molecular dynamics simulations, which demonstrates that graphene maintains nonlinear elasticity prior to the failure strain, and find Young's modulus has strong strain range dependence. Thus, the elastic region of the tensile curve can be divided into the linear elastic region and nonlinear elastic region, and the linear elastic limit strains for the armchair and zigzag graphene are about 2.5% and 1.5% regardless of size. What is more, Young's modulus is dependent on the chiral angle but is not sensitive to size. The failure strain and fracture strength are not only dependent on the chiral angle but also have obvious size effects. As the size range and size ratio increase, the failure strain and fracture strength show a decreasing trend.

**Code availability** The code required to reproduce these findings cannot be shared at this time due to technical or time limitations.

**Data availability** The raw/processed data required to reproduce these findings cannot be shared at this time due to technical or time limitations.

**Author contribution** Yi-Xiu Du: Methodology, Investigation, Validation, Writing - original draft, Writing - review & editing. Li-Jun Zhou: Conceptualization, Methodology, Validation, Writing - review & editing, Supervision. Jian-Gang Guo: Methodology, Investigation, Validation, Writing - review & editing, Funding acquisition.

**Funding** This work was financially supported by the National Natural Science Foundation of China (Grant no. 11872268), the Innovative Group Project of National Natural Science Foundation of China (Grant no. 12021002) and the Major Program of National Natural Science Foundation of China (Grant no. 11890682).

## Declarations

**Ethics approval** Not applicable.

**Consent to participate** Not applicable.

**Consent for publication** Not applicable.

**Conflict of interest** The authors declare no competing interests.

## References

1. Novoselov KS, Geim AK, Morozov SV et al (2004) Electric field in atomically thin carbon films. *Science* 306:666–669.
2. Ramanathan T, Abdala AA, Stankovich S et al (2008) Functionalized graphene sheets for polymer

- nanocomposites. *Nat Nanotechnol* 3:327–331.
3. Young RJ, Kinloch IA, Gong L, Novoselov KS (2012) The mechanics of graphene nanocomposites: A review. *Compos Sci Technol* 72:1459–1476.
  4. Lee C, Wei X, Kysar JW, Hone J (2008) Measurement of the elastic properties and intrinsic strength of monolayer graphene. *Science* 321:385–388.
  5. Geim AK (2009) Graphene: Status and prospects. *Science* 324:1530–1534.
  6. Cadelano E, Palla PL, Giordano S, Colombo L (2009) Nonlinear elasticity of monolayer graphene. *Phys Rev Lett* 102:1–4.
  7. Bu H, Chen Y, Zou M et al (2009) Atomistic simulations of mechanical properties of graphene nanoribbons. *Phys Lett Sect A Gen At Solid State Phys* 373:3359–3362.
  8. Ni Z, Bu H, Zou M et al (2010) Anisotropic mechanical properties of graphene sheets from molecular dynamics. *Phys B Condens Matter* 405:1301–1306.
  9. Zhao H, Aluru NR (2010) Temperature and strain-rate dependent fracture strength of graphene. *J Appl Phys* 108:064321.
  10. Mortazavi B, Rémond Y, Ahzi S, Toniazzi V (2012) Thickness and chirality effects on tensile behavior of few-layer graphene by molecular dynamics simulations. *Comput Mater Sci* 53:298–302.
  11. Zhao H, Min K, Aluru NR (2009) Size and chirality dependent elastic properties of graphene nanoribbons under uniaxial tension. *Nano Lett* 9:3012–3015.
  12. Zhang YY, Gu YT (2013) Mechanical properties of graphene: Effects of layer number, temperature and isotope. *Comput Mater Sci* 71:197–200.
  13. Pei QX, Zhang YW, Shenoy VB (2010) A molecular dynamics study of the mechanical properties of hydrogen functionalized graphene. *Carbon N Y* 48:898–904.
  14. Sun YJ, Huang YH, Ma F et al (2014) Molecular dynamics simulation on double-elastic deformation of zigzag graphene nanoribbons at low temperature. *Mater Sci Eng B Solid-State Mater Adv Technol* 180:1–6.
  15. Wang L, Zhang Q (2012) Elastic behavior of bilayer graphene under in-plane loadings. *Curr Appl Phys* 12:1173–1177.
  16. López-Polín G, Jaafar M, Guinea F et al (2017) The influence of strain on the elastic constants of graphene. *Carbon N Y* 124:42–48.
  17. Androulidakis C, Tsoukleri G, Koutroumanis N et al (2015) Experimentally derived axial stress-strain relations for two-dimensional materials such as monolayer graphene. *Carbon N Y* 81:322–328.
  18. Prabhakar S, Melnik R (2019) Ab-initio calculations of strain induced relaxed shape armchair graphene nanoribbon. *Phys E Low-Dimensional Syst Nanostructures* 114:113648.
  19. Qu LH, Zhang JM, Xu KW, Ji V (2015) A first-principles study on uniaxial strain effects of nonplanar oxygen-functionalized armchair graphene nanoribbons. *J Alloys Compd* 631:219–224.
  20. Los JH, Fasolino A, Katsnelson MI (2016) Scaling Behavior and Strain Dependence of In-Plane Elastic Properties of Graphene. *Phys Rev Lett* 116:1–5.
  21. Hosseini Kordkheili SA, Moshrefzadeh-Sani H (2013) Mechanical properties of double-layered graphene sheets. *Comput Mater Sci* 69:335–343.
  22. Wang SP, Guo JG, Jiang Y (2013) The size- and chirality-dependent elastic properties of graphene nanofilms. *J Comput Theor Nanosci* 10:250–256.
  23. Georgantzinos SK, Giannopoulos GI, Katsareas DE et al (2011) Size-dependent non-linear

- mechanical properties of graphene nanoribbons. *Comput Mater Sci* 50:2057–2062.
24. Giannopoulos GI, Liosatos IA, Moukanidis AK (2011) Parametric study of elastic mechanical properties of graphene nanoribbons by a new structural mechanics approach. *Phys E Low-Dimensional Syst Nanostructures* 44:124–134.
  25. Shen L, Shen HS, Zhang CL (2010) Temperature-dependent elastic properties of single layer graphene sheets. *Mater Des* 31:4445–4449.
  26. Chen MQ, Quek SS, Sha ZD et al (2015) Effects of grain size, temperature and strain rate on the mechanical properties of polycrystalline graphene - A molecular dynamics study. *Carbon N Y* 85:135–146.
  27. Azimi Resketi N, Ahmadi Amiri H, Dehestani M (2018) Effects of Size and Shape on Elastic Constants of Graphene Sheet. *Structures* 13:131–138.
  28. Yanovsky YG, Nikitina EA, Karnet YN, Nikitin SM (2010) Simulation of deformation and fracture of graphene: Effect of size, defects and surface modification. *Phys Mesomech* 13:329–336.
  29. Zhang Y, Liu L, Xi N et al (2014) Friction anisotropy dependence on lattice orientation of graphene. *Sci China Physics, Mech Astron* 57:663–667.
  30. Tao C, Jiao L, Yazyev OV et al (2011) Spatially resolving edge states of chiral graphene nanoribbons. *Nat Phys* 7:616–620.
  31. Stuart SJ, Tutein AB, Harrison JA (2000) A reactive potential for hydrocarbons with intermolecular interactions. *J Chem Phys* 112:6472–6486.
  32. He L, Guo S, Lei J et al (2014) The effect of Stone-Thrower-Wales defects on mechanical properties of graphene sheets - A molecular dynamics study. *Carbon N Y* 75:124–132.
  33. Wang Y, Lei J, Liu Z (2019) Molecular dynamics study on the anisotropic Poisson's ratio of the graphene. *Diam Relat Mater* 93:66–74.
  34. Zheng Y, Xu L, Fan Z et al (2012) Mechanical Properties of Graphene Nanobuds: A Molecular Dynamics Study. *Curr Nanosci* 8:89–96.
  35. Fasolino A, Los JH, Katsnelson MI (2007) Intrinsic ripples in graphene. *Nat Mater* 6:858–861.
  36. Jin Y, Yuan FG (2003) Simulation of elastic properties of single-walled carbon nanotubes. *Compos Sci Technol* 63:1507–1515.
  37. Nayebi P, Zaminpayma E (2016) A molecular dynamic simulation study of mechanical properties of graphene-polythiophene composite with Reax force field. *Phys Lett Sect A Gen At Solid State Phys* 380:628–633.
  38. Du H, Xue T, Xu C et al (2018) Improvement of mechanical properties of graphene/substrate interface via regulation of initial strain through cyclic loading. *Opt Lasers Eng* 110:356–363.
  39. Liu X, He X, Sun L et al (2020) A chirality-dependent peridynamic model for the fracture analysis of graphene sheets. *Mech Mater* 149:103535.
  40. Hossain MZ, Ahmed T, Silverman B et al (2018) Anisotropic toughness and strength in graphene and its atomistic origin. *J Mech Phys Solids* 110:118–136.
  41. Yin H, Qi HJ, Fan F et al (2015) Griffith criterion for brittle fracture in graphene. *Nano Lett* 15:1918–1924.